iScience

CellPress
OPEN ACCESS

Article

NF1-dependent disruption of the blood-nerve-barrier is improved by blockade of P2RY14

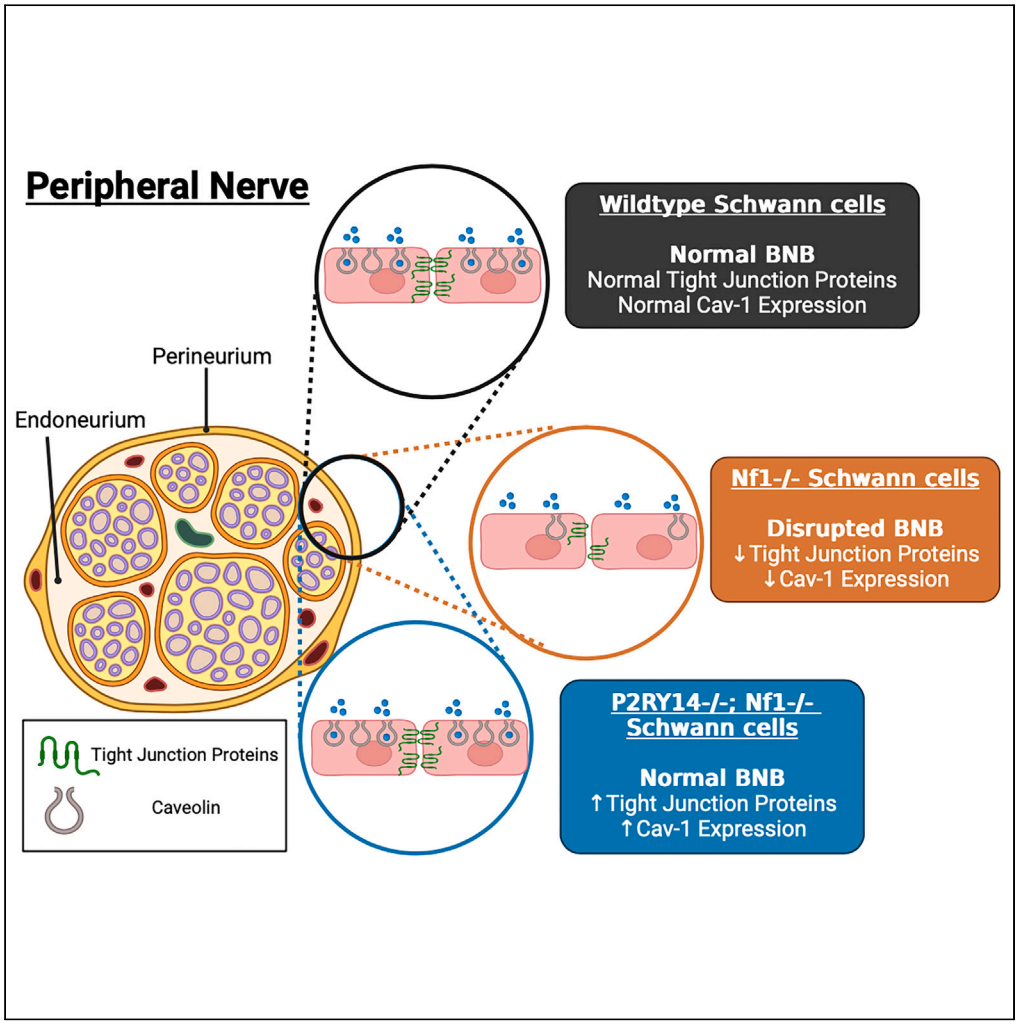

Jennifer Patritti-Cram, Eric P. Rahrmann, Tilat A. Rizvi, Katherine C. Scheffer, Timothy N. Phoenix, David A. Largaespada, Nancy Ratner

nancy.ratner@cchmc.org

Highlights

In human and mouse neurofibromas the blood-nerve-barrier (BNB) is leaky

Nf1 loss in Schwann cells (SCs) decreases BNB: ZO-1, tight junctions and *Cav1*

Loss of *Cav1* promotes BNB disruption and tumors when RAS is elevated in SCs

We define P2RY14 as a targetable receptor that can rescue BNB function in NF1

Patritti-Cram et al., iScience *27*, 110294
July 19, 2024
https://doi.org/10.1016/j.isci.2024.110294

iScience

CellPress
OPEN ACCESS

Article

NF1-dependent disruption of the blood-nerve-barrier is improved by blockade of P2RY14

Jennifer Patritti-Cram,[1,2] Eric P. Rahrmann,[3] Tilat A. Rizvi,[1] Katherine C. Scheffer,[1] Timothy N. Phoenix,[4] David A. Largaespada,[5] and Nancy Ratner[1,6,7,*]

SUMMARY

The blood-nerve-barrier (BNB) that regulates peripheral nerve homeostasis is formed by endoneurial capillaries and perineurial cells surrounding the Schwann cell (SC)-rich endoneurium. Barrier dysfunction is common in human tumorigenesis, including in some nerve tumors. We identify barrier disruption in human *NF1* deficient neurofibromas, which were characterized by reduced perineurial cell glucose transporter 1 (GLUT1) expression and increased endoneurial fibrin(ogen) deposition. Conditional *Nf1* loss in murine SCs recapitulated these alterations and revealed decreased tight junctions and decreased caveolin-1 (*Cav1*) expression in mutant nerves and in tumors, implicating reduced *Cav1*-mediated transcytosis in barrier disruption and tumorigenesis. Additionally, elevated receptor tyrosine kinase activity and genetic deletion of *Cav1* increased endoneurial fibrin(ogen), and promoted SC tumor formation. Finally, when SC lacked *Nf1*, genetic loss or pharmacological inhibition of P2RY14 rescued *Cav1* expression and barrier function. Thus, loss of *Nf1* in SC causes dysfunction of the BNB via P2RY14-mediated G-protein coupled receptor (GPCR) signaling.

INTRODUCTION

The blood-nerve-barrier (BNB) plays a crucial role in maintaining the homeostatic balance between the peripheral nervous system and the systemic circulation, safeguarding the neural environment from potential harm. Normal peripheral nerves contain nerve axons and supporting Schwann cells (SCs), and endothelial cell-lined capillaries which are part of the BNB (Figure 1A).[1,2] The endoneurial compartment is surrounded by an additional barrier comprised layers of specialized perineurial cells that regulate diffusion through tight junctions and small flask-shaped membrane vesicles called caveolae, in a process called transcytosis.[3–7] Pathological breakdown of the perineurium barrier, such as by nerve injury, disrupts nerve homeostasis, correlating with entry of serum factors and infiltration of immune cells into the endoneurium that can lead to neuropathy.[5,8,9,10] Perineurium disruption is a feature of injury-induced neuromas and some nerve tumors, including schwannomas and cutaneous neurofibromas.[11,12]

Plexiform neurofibromas (PNFs) are tumors that grow within nerves and are a feature of individuals with neurofibromatosis type 1 (NF1), in which loss of *NF1* in SCs elevates RAS-MAPK signaling downstream of receptor tyrosine kinase signaling and affects cAMP signaling.[13] PNFs are said to show an altered perineurium and sometimes invade adjacent tissue.[12,14,15] However, immunohistochemical analysis of five plexiform neurofibromas previously showed low serum protein deposition in the endoneurium,[12] leaving the status of the perineurium uncertain in this setting. Here, we studied the pathology of the BNB in NF1 patient's plexiform neurofibroma tumors and in our laboratory's well-characterized mouse model of NF1 associated plexiform neurofibroma, in which genetic deletion of *Nf1* in Schwann cells drives inflammation and fibrosis in peripheral nerves and the formation of paraspinal plexiform neurofibromas (PNF). In this *Nf1* mouse model, invasion of immune cells, largely macrophages, occurs and precedes tumor formation.[16,17] The BNB has been poorly studied in either NF1 tumors and, indeed, in many nerve pathologies.

An especially understudied aspect of peripheral nerve is the caveolae-mediated active transport through the cytoplasm of barrier cells. Caveolae are non-clathrin-coated vesicular invaginations that pinch-off from the plasma membranes of cells. Caveolin-1 (Cav1) is the major protein constituent of caveolae, and increased *Cav1* expression can stimulate transcytosis and thus permeability.[18] However, loss of *Cav1* is

[1]Division of Experimental Hematology and Cancer Biology, Cancer & Blood Diseases Institute, Cincinnati Children's Hospital Medical Center, Cincinnati, OH 45229, USA
[2]Neuroscience Graduate Program, University of Cincinnati College of Medicine, Cincinnati, OH 45267-0713, USA
[3]Cancer Research UK Cambridge Institute, University of Cambridge, Cambridge, UK
[4]Division of Pharmaceutical Sciences, James L. Wrinkle College of Pharmacy, University of Cincinnati, Cincinnati, OH 45229, USA
[5]Department of Pediatrics, Masonic Cancer Center, University of Minnesota, Minneapolis, MN 55455, USA
[6]Department of Pediatrics, University of Cincinnati College of Medicine, Cincinnati, OH 45267, USA
[7]Lead Contact
*Correspondence: nancy.ratner@cchmc.org
https://doi.org/10.1016/j.isci.2024.110294

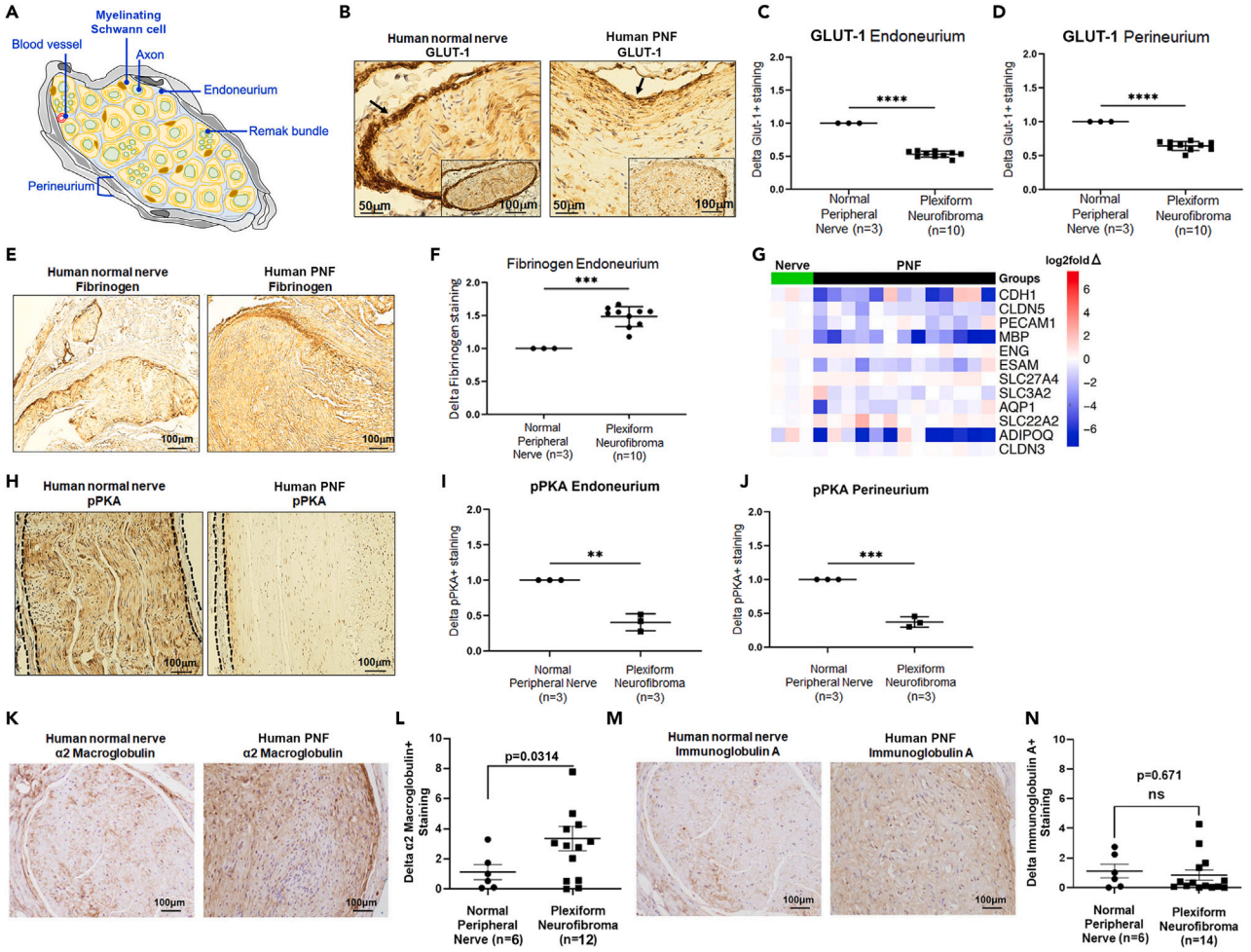

Figure 1. Human PNFs have a disrupted BNB with reduced GLUT-1 staining and fibrinogen deposition

(A) Schematic of cross-section of normal peripheral nerve. The perineurium surrounds the endoneurium, containing axons and Schwann cells (small axons are collected into Remak bundles; large axons are myelinated) and endoneurial capillaries (blood vessel).

(B) Anti-GLUT-1 immunostaining of normal human peripheral nerve and plexiform neurofibroma sections (DAB staining: brown (black arrows point to the perineurium) (normal human peripheral nerve $n = 3$; plexiform neurofibroma $n = 10$).

(C) Quantification of GLUT1+ staining in the endoneurium (Student's t test; **** = $p < 0.0001$) (normal human peripheral nerve $n = 3$; plexiform neurofibroma $n = 10$).

(D) Quantification of GLUT1+ staining in the perineurium (Student's t test; **** = $p < 0.0001$) (normal human peripheral nerve $n = 3$; plexiform neurofibroma $n = 10$).

(E) Anti-fibrin/fibrinogen immunostaining of normal human peripheral nerve and plexiform neurofibroma sections (DAB staining: brown) (normal human peripheral nerve $n = 3$; plexiform neurofibroma $n = 10$).

(F) Quantification of fibrinogen/fibrin in the endoneurium (Student's t test; ***$p = 0.0002$) (normal human peripheral nerve $n = 3$; plexiform neurofibroma $n = 10$).

(G) Whole-transcriptome analysis in normal human peripheral nerve and plexiform neurofibroma tumor tissue showing reduced expression of BBB/BNB genes *Cldn-5*, *Aqp1*, *Adipoq*, and *Cldn3*.

(H) Normal human peripheral nerve and plexiform neurofibroma tumor sections stained with anti-PKA-P-substrate (DAB staining: brown) showing reduced staining in PNF (normal human peripheral nerve $n = 3$; plexiform neurofibroma $n = 3$).

(I) Quantification of pPKA in the endoneurium (Student's t test; **$p = 0.0010$) (normal human peripheral nerve $n = 3$; plexiform neurofibroma $n = 3$).

(J) Quantification of pPKA in the perineurium (Student's t test; ***$p = 0.0002$) (normal human peripheral nerve $n = 3$; plexiform neurofibroma $n = 3$).

(K) α2 macroglobulin staining in normal human peripheral nerve and plexiform neurofibroma tumors. (normal human peripheral nerve $n = 6$; plexiform neurofibroma $n = 12$).

(L) Quantification of α2 macroglobulin staining in normal human peripheral nerve and plexiform neurofibroma tumors (Student's t test, n.s $p = 0.1031$) (normal human peripheral nerve $n = 6$; plexiform neurofibroma $n = 12$).

(M) IgA staining in normal human peripheral nerve and plexiform neurofibroma tumor. (normal human peripheral nerve $n = 6$; plexiform neurofibroma $n = 14$).

(N) Quantification of IgA staining in normal human peripheral nerve and plexiform neurofibroma tumor. (Student's t test, n.s $p = 0.671$) (normal human peripheral nerve $n = 6$; plexiform neurofibroma $n = 14$).

known to also increase permeability in the blood brain barrier.[19] Caveolin function may therefore differ based on cell specificity and physiological context, including in the nerve/tumor microenvironment. In perineurial cells, caveolae function is to transport substances toward, and possibly also away from, the endoneurium.[20] Caveolin is known to inhibit downstream activation signals inside cells, including H-Ras, MAPK, eNOS, and c-Src.[21–24] In addition, caveolin binds Gαq-GDP and PKA, resulting in inhibition of PKA signaling. Thus, endothelial cells lacking *Cav1* increase intracellular cAMP levels.[25,26] As caveolin controls intracellular signaling pathways that regulate cell survival, proliferation, and intracellular transport, it has been hypothesized that perturbations in *Cav1* expression and/or function play important roles in human disease.[6,27] Here, we explore the role that *Cav1* plays in the BNB.

Cav1 is also known to be regulated by purinergic receptors.[28] However, in mammals, purinergic receptors play dichotomous roles. Activation of some purinergic receptors stabilizes endothelial barrier function, while chronic activation of other purinergic receptors disrupts barrier function.[29–34] Activation of purinergic signaling occurs under pathological conditions when nucleotides (e.g., ATP, UTP, adenosine) are released from injured cells and activate purinergic GPCRs on nearby cells modulate intracellular cAMP signaling, and other pathways linked to changes in barrier function.[35] The relationship is complex. For example, increasing adenosine levels leads to increases in mouse blood-brain-barrier (BBB) permeability,[36] yet protects against development of brain edema and leukocyte infiltration.[37] Here, we studied the purinergic receptor P2RY14. P2RY14 is a UDP-glucose receptor that signals through G_i to inhibit adenylate cyclase and decrease intracellular levels of cAMP.[38] P2RY14-RAS pathway crosstalk also results in altered RAS signaling in the context of *Nf1* loss in Schwann cells.[39] In brain microvascular endothelial cells that express P2RY14, receptor activation induces a pro-inflammatory response.[40]

Here, we tested the hypothesis that P2RY14, and/or caveolin, regulate BNB function after loss of *Nf1* in SCs. We show that in human plexiform neurofibroma tumors and in a mouse model of NF1, that the BNB in the peripheral nerves and neurofibroma tumors is leaky. These findings are supported by increased fibrin(ogen) in the endoneurium. We also found that *Nf1* loss in SCs also decreases BNB components associated with a restrictive barrier including reduced organization of Z01 and the absence of morphologically defined tight junctions (TJs) in perineurial cells, and decreased *Cav1* expression and morphologically defined caveolae. Notably, genetic loss of *Cav1* was sufficient to promote barrier disruption, and tumor formation, when receptor tyrosine kinase-driven RAS signaling was elevated in SCs. Finally, we conclude that genetic and pharmacological approaches define P2RY14 as a targetable receptor that can rescue BNB function in NF1.

RESULTS

Human plexiform neurofibromas have a disrupted BNB

In the normal nerve, Schwann cells, axons, and capillaries in the endoneurium are surrounded by a perineurium comprised fibroblast-like cells connected by tight junctions (schematic, Figure 1A). To determine the status of the perineurium, we first evaluated the expression of glucose transporter 1 (GLUT1), a marker of barrier integrity, in tissue sections of normal human nerve and PNF tumors.[14,41,42] Anti-GLUT1 immunoreactivity was significantly reduced (2-fold) in both the endoneurium and the perineurium in PNF tumors versus normal nerve (Figures 1B–1D). To assess if the BNB was disrupted and caused a "leaky" phenotype, we stained adjacent sections with anti-fibrinogen/fibrin. Fibrinogen is a serum protein normally excluded by intact barriers.[43] Human PNFs showed a significant (2-fold) increase in fibrin deposition in the endoneurium, compared to normal nerve (Figures 1E and 1F). Whole-transcriptome analysis in human peripheral nerve from normal individuals, versus PNF from individuals with NF1, revealed reduced expression of known BBB and BNB genes including *CLDN5, AQP1, ADIPOQ*, and *CLDN3* (Figure 1G). We also measured cAMP-dependent protein kinase A (PKA) in the human normal peripheral nerve and in human PNFs, as cAMP-pPKA is known to be required for formation and maintenance of barrier integrity in many systems.[32,44] PKA substrate phosphorylation (using anti *p*-PKA substrate antibody) was used as an indirect readout of cAMP levels. Compared to human normal peripheral nerve, PNFs showed significantly reduced *p*-PKA substrate expression in both the tumor endoneurium and the perineurium (Figure 1H–J).

Next, to understand to what extent the BNB is disrupted in PNFs, we tested if high molecular weight proteins α2 macroglobulin (MW = 820,000 kd) and immunoglobulin A (MW = 900,000) are present in the endoneurium. The presence of these molecules correlates to the level of "leakiness" of the nerve barriers.[45,46] Staining with anti-α2 macroglobulin was significantly (*$p = 0.0314$) increased in most human neurofibromas versus nerve (Figures 1K and 1L). In contrast, staining with anti-immunoglobulin A did not differ between PNFs and normal nerve ($p = 0.671$); Figures 1M and 1N). These results show that fibrinogen marks the leak in neurofibromas, and that some plexiform neurofibroma tumors also show striking leakage of the high molecular weight protein α2 macroglobulin. Thus, the BNB is compromised in plexiform neurofibroma tumors, and the degree of "leakiness" varies among tumors.

The BNB is disrupted in a mouse model of NF1

To understand if the BNB disruption is occurring due to the physical presence a tumor mass or due to altered cellular signaling processes, we decided to assess the BNB in the peripheral nerves of a well-characterized mouse model of NF1.[47] In this mouse model, Cre recombinase is expressed from desert hedgehog (*Dhh*) regulatory sequences to genetically delete the conditionally expressed *Nf1* allele (*Nf1fl/fl*) in developing SCs at embryonic day 12.5.[47] Peripheral nerves, independent of tumor formation, become abnormal in this model, showing loss of axon-SC interaction in Remak bundles, mast cell, and macrophage accumulation, and nerve fibrosis.[17] *Nf1fl/fl;Dhh+* mice develop cervical paraspinal PNFs by 4-month of age. PNF tumors enlarge over time, compressing the spinal cord and causing paralysis, with mice necessitating sacrifice beginning around 7-month of age.[47]

We assessed nerve structure in semi-thin sections in *WT* and *Nf1fl/fl;Dhh+* mice saphenous nerve and sciatic nerve, where tumors do not form. *WT* mice present organized perineurium morphology in both semi-thin section and in electron micrographs (EM); no striking alterations were observed in *Nf1fl/fl;Dhh+* mutant nerves (Figure 2A). Neither perineurial width nor numbers of perineurial layers were significantly

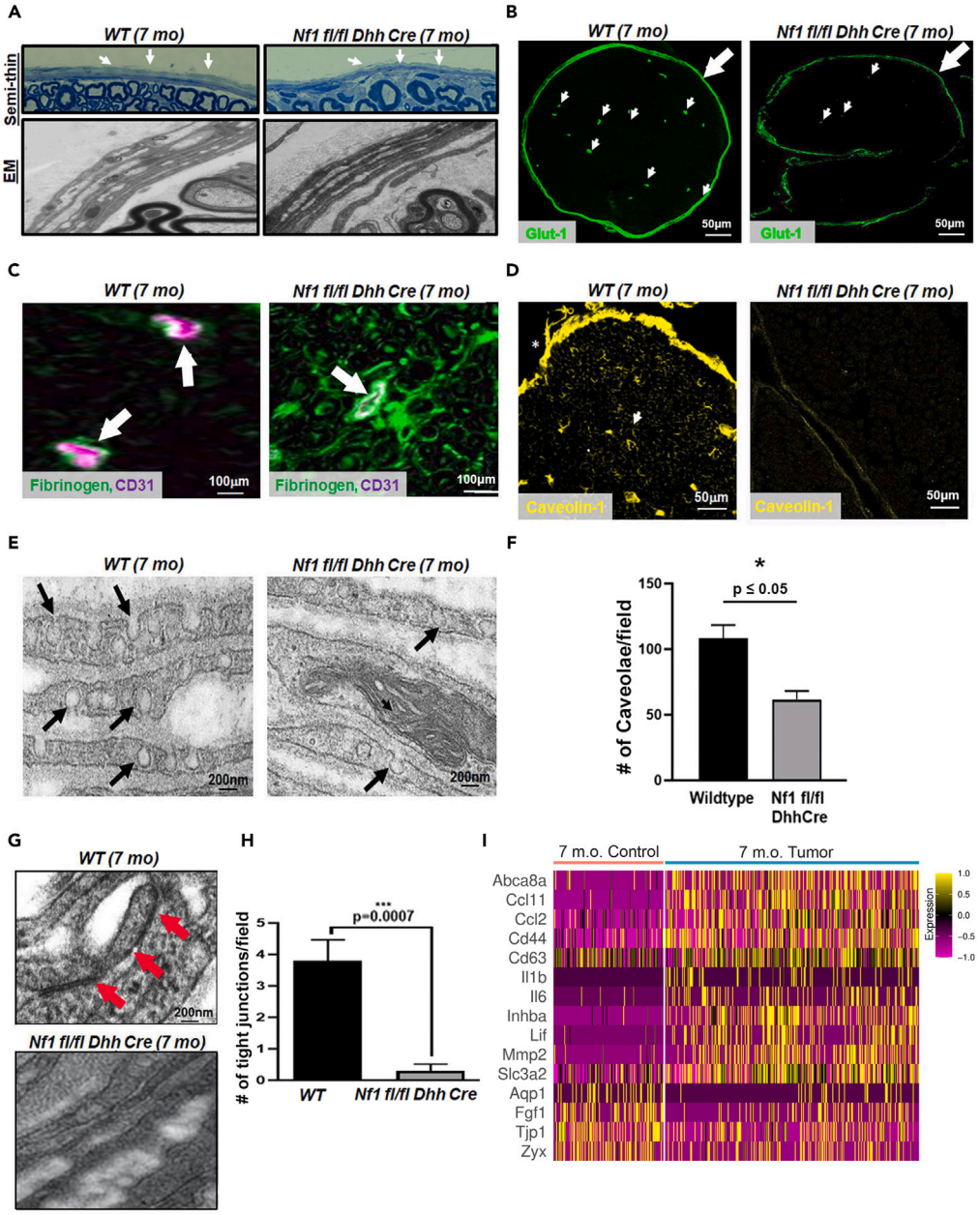

Figure 2. Nf1fl/fl; Dhh+ mice have disrupted BNB, decreased TJ numbers, increased fibrinogen deposition, and reduced caveolin

(A) Top, saphenous nerve semi-thin sections 7-month *WT* and *Nf1fl/fl;Dhh+* (arrows point to the perineurium). Bottom, electron micrographs showing a similar area.

(B) Anti-Glut1 staining in 7-month *WT* and *Nf1fl/fl;Dhh+* sciatic nerve (large arrow indicates the perineurium; small arrows indicate Glut1+ endoneurial capillaries; *WT* $n = 3$; *Nf1 fl/fl Dhh+* $n = 3$).

(C) Anti-fibrinogen (green) and anti-CD31 (purple) staining (arrows point to $CD31^+$ endoneurial capillaries) in 7-month *WT* and *Nf1fl/fl;Dhh+* sciatic nerve. (*WT* $n = 3$; *Nf1 fl/fl Dhh+* $n = 3$).

(D) Anti-Caveolin antibody staining in 7-month *WT* and *Nf1fl/fl;Dhh+* sciatic nerve. (*WT* $n = 3$; *Nf1 fl/fl Dhh+* $n = 3$).

(E) Electron micrograph showing caveolae in perineurial cells in 7-month *WT* and *Nf1fl/fl;Dhh+* saphenous nerve (black arrows show caveolae invaginating and inside perineurial cells) (*WT* normal nerve $n = 3$; *Nf1fl/fl;Dhh+* plexiform neurofibroma $n = 3$).

(F) Quantification caveolae per field of view in 7-month *WT* and *Nf1fl/fl;Dhh+* saphenous nerve (Student's t test,*$p \leq 0.05$) (*WT* normal nerve $n = 3$; *Nf1fl/fl;Dhh+* plexiform neurofibroma $n = 3$).

Figure 2. *Continued*

(G) Electron micrograph showing TJs between perineurial cells in 7-month *WT* and *Nf1fl/fl;Dhh+* saphenous nerve. Red arrows highlight a tight junction in a in 7-month *WT* saphenous nerve perineurium; TJs are largely missing between perineurial cells in mutant nerve (*WT* normal nerve $n = 3$; *Nf1fl/fl;Dhh+* plexiform neurofibroma $n = 3$).

(H) Quantification of tight junctions per field of view in 7-month *WT* and *Nf1fl/fl;Dhh+* saphenous nerve (Student's t test,***$p = 0.0007$) (*WT* normal nerve $n = 3$; *Nf1fl/fl;Dhh+* nerve $n = 3$).

(I) Heatmap of gene expression in single perineurial cells from 7-month mice wild type nerve/dorsal root ganglia and plexiform neurofibroma tumor, using RNA-Seq.

altered in saphenous nerve sections (Figure S1A). However, *Nf1fl/fl;Dhh+* mice perfused with a 10kDa blue dextran showed a slight leak of blue dextran into the nerve endoneurium in 7-month-old mice which was not observed in controls, suggesting a compromised BNB (Figure S2C). Minor accumulation of dextrans is consistent with robust, rapid, uptake into nerve macrophages.[3]

We evaluated BNB integrity by assessing GLUT-1 and fibrinogen expression. *Nf1fl/fl;Dhh+* mice showed reduced and patchy GLUT-1 expression in endoneurial capillaries (small arrows) and perineurial cells (large arrow) relative to *WT* control mice (Figure 2B), consistent with disrupted barrier function. We also assessed the expression of tight junctions in these mice. Staining of *WT* and *Nf1fl/fl;Dhh+* tissue sections with antibodies recognizing a major tight junction protein, Z0-1 revealed disorganized tight junctions in *Nf1fl/fl;Dhh+* mice, similarly consistent with disrupted barrier function (Figure S1B). Importantly, fibrinogen immunoreactivity was strikingly increased in the endoneurium of *Nf1fl/fl;Dhh+* nerves versus wild type controls (Figure 2C). $CD31^+$ endoneurial vessel number was not significantly changed in *Nf1fl/fl;Dhh+* mice compared to *WT* control mice (Figure 2C and Figure S1C).

To test if transcytosis might be affected by *Nf1* loss in Schwann cells, we immunostained *WT* and *Nf1fl/fl;Dhh+* sciatic nerves with anti-caveolin1 (CAV-1). CAV-1 staining, which was robust in the control perineurium and endoneurium, was dramatically reduced in *Nf1fl/fl;Dhh+* nerve (Figure 2D). Quantification of caveolae per field of view at the electron micrograph level in saphenous nerve verified this result (Figures 2E and 2F). To determine if tight junctions are also affected, we quantified TJ in saphenous nerve electron micrographs. *WT* nerve showed numerous TJs in the perineurium, but TJs were difficult to identify in *Nf1fl/fl;Dhh+* nerve (Figure 2G). Quantification verified a reduction of TJs in the perineurium of *Nf1fl/fl;Dhh+* nerves versus *WT* controls (Figure 2H). Single cell RNA sequencing analysis of perineurial cells from WT control and *Nf1 fl/fl Dhh+* neurofibromas obtained from existing data (GEO Accession #181985), verified perineurial cell de-regulation of BNB-related gene expression, including decreased expression of *Aqp1*, *Fgf1*, *the Tjp1*, and increased expression of *Il1b* (Figure 2I). These results indicate that, as in human tumors, the genetic deletion of *Nf1* in Schwann cells compromises the BNB. These phenotypes occur in nerve, in the absence of tumor formation and correlated with altered perineurial cell gene expression and reduced numbers of both TJs and caveolae in *Nf1fl/fl;Dhh+* perineurial cells.

Loss of *Cav-1* increases BNB permeability when RTK signaling is increased in Schwann cells

The decrease in caveolin expression seen in *Nf1fl/fl;Dhh+* mice nerve was of interest to us because caveolin is known to modulate RAS and cAMP signaling relevant to NF1. Also, we had previously identified *Cav1* as a putative tumor suppressor gene in a transposon-mediated mutagenesis screen for neurofibroma formation.[48] Therefore, we analyzed in more detail the mutagenic transposon insertions into the *Cav1* gene from neurofibroma samples and found that each insertion predicted either loss of function through disruption of transcription (5/8) or expression of a truncated transcript (3/8) (Figure 3A). We then analyzed existing microarray data (GEO Accession # GSE14038) and found that *Cav1* expression was significantly reduced in mouse models of NF1-associated PNF when compared to normal mouse nerves (****$p < 0.05$) (Figure 3B). Therefore, we tested if deletion of *Cav1* would exacerbate BNB disruption induced by elevated RTK signaling in Schwann cells. *CNPase-hEGFR* transgenic mice express the human epidermal growth factor receptor (hEGFR) in SCs in peripheral nerve.[49] Nerves show Remak bundle disruption and nerve fibrosis characteristic of human PNF, but tumors form in only 5% of mice.[49] *CNPase-hEGFR;*$Cav1^{+/-}$ mice showed increased fibrinogen expression in the endoneurium, which was further elevated as compared to either mutant alone (Figure 3C; 3D). However, GLUT-1 expression did not change significantly in these mice (data not shown).

cAMP is known to play a role in integrity of barriers which can be regulated by caveolin. Previously, it has been shown that PKA substrate staining, an indirect measure of cAMP/PKA activity is reduced in *Nf1fl/fl;Dhh+* SCs.[39] Here, we found that in nerves from *CNPase-hEGFR* mice, *p*-PKA substrate staining was also decreased relative to control, but was rescued in *CNPase-hEGFR;*$Cav1^{+/-}$ double mutants (Figures 3E and 3F). Thus, when *Cav1* expression is reduced, EGFR-mediated signals correlate with normalized cAMP levels, yet enables barrier dysfunction. This result implies that reducing cAMP correlates with, but is not necessary, for barrier dysfunction. Rather, as reducing *Cav1* also increases signaling through RTKs, including EGFR,[21,50] we hypothesize that increased tyrosine kinase signaling accounts for the increased leak in double mutants.

EGFR mice are predisposed to PNF formation and transformation to malignant peripheral nerve sheath tumors (MPNST), as observed with increasing EGFR gene dosage[51] or breeding to mice lacking certain tumor suppressor genes.[48,52] In $Cav1^{-/-}$ mice crossed to CNPase-hEGFR transgenic mice, there was a significant increase in the size of the paraspinal dorsal root ganglia (DRG) of *CNPase-hEGFR;*$Cav1^{+/-}$ and *CNPase-hEGFR;*$Cav1^{-/-}$ mice compared to the littermate controls by 7-month of age, consistent with neurofibroma formation (Figures S4A and 4B). Histological analysis showed that loss of *Cav1* (in at least one allele) resulted in disorganized nerve morphology characteristic of PNFs, exemplified by H&E and S100 staining (Figure S4C,4D). Based on these data, we conclude that in peripheral nerves, in addition to its role in barrier maintenance, *Cav1* acts as a tumor suppressor.

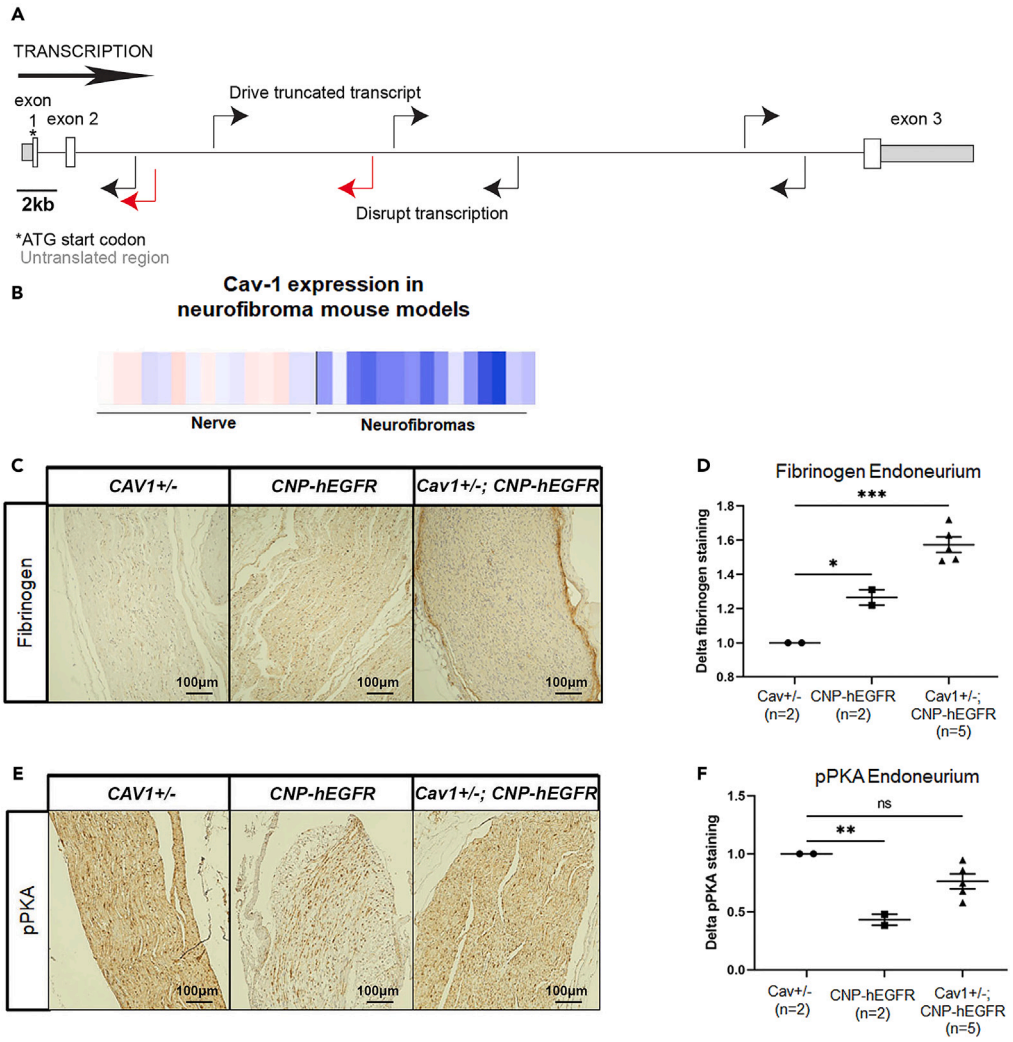

Figure 3. Loss of one allele of Cav1 in CNPase-*h*EGFR mice causes fibrin deposition and rescues low P-PKA caused by EGFR alone

(A) Schematic of T2/Onc insertion sites within the Cav1 gene from an SB screen for neurofibroma (black arrows) and grade 3 PNSTs (red arrows). The direction of gene transcription is left to right. Arrow heads represent the direction of the MSCV 5′ LTR promoter region within T2/Onc compared to the direction of gene transcription. The schematic predicts that Cav1 expression is disrupted in SB-induced tumors.

(B) Analysis of microarray expression of *Cav1* in neurofibroma tumors from diverse mouse models versus nerves from littermate mice (nerve) shows reduced *Cav1* mRNA expression in PNF (****$p < 0.05$).

(C) Anti-fibrinogen/fibrin staining in sciatic nerve sections from *Cav1*$^{+/-}$, *CNPase-hEGFR and Cav1*$^{+/-}$,*CNPase-hEGFR* mice. (*Cav1*$^{+/-}$ *n* = 2; *CNP-hEGFR n* = 2; *Cav1*$^{+/-}$ *CNP-hEGFR n* = 5).

(D) Quantification of anti-fibrinogen/fibrin staining in sciatic nerve sections (*$p = 0.0376$; ***$p = 0.0004$) (*Cav+/– n* = 2; *CNP-hEGFR n* = 2; *Cav1*$^{+/-}$ *CNP-hEGFR n* = 5).

(E) Anti-P-PKA substrate staining in sciatic nerve sections from *Cav1*$^{+/-}$, *CNPase-hEGFR and Cav1*$^{+/-}$,*CNPase-hEGFR* mice. (*Cav1*$^{+/-}$ *n* = 2; *CNP-hEGFR n* = 2; *Cav1*$^{+/-}$ *CNP-hEGFR n* = 5).

(F) Quantification of anti-P-PKA substrate staining in sciatic nerve sections from *Cav1*$^{+/-}$, *CNPase-hEGFR and Cav1*$^{+/-}$,*CNPase-hEGFR* mice (**$p = 0.0190$) (*Cav+/– n* = 2; *CNP-hEGFR n* = 2; *Cav1*$^{+/-}$ *CNP-hEGFR n* = 5). Statistics: one-way ANOVA in all panels.

P2ry14 deletion in *Nf1fl/fl;Dhh+* mice restore BNB morphology, reduces fibrinogen deposition and rescues Cav1 expression

G-protein coupled receptor signaling also modulates both cAMP and RTK downstream signaling. We hypothesized that GPCR signaling in *Nf1fl/fl;Dhh+* nerve might contribute to reduced caveolin and increased BNB permeability in NF1. Purinergic receptor P2RY14 inhibits adenylate cyclase and reduces intracellular levels of cAMP. We recently found that this purinergic receptor is a critical regulator of cAMP levels in *Nf1fl/fl;Dhh+* endoneurial SCs.[39] To test whether *P2ry14* has effects on the BNB in the context of NF1 loss, we generated *P2ry14*$^{-/-}$;*Nf1fl/fl;Dhh+* mice. In *P2ry14*$^{-/-}$ mice, most of the coding region of *P2ry14* is replaced by a β-galactosidase (β-gal) cassette, so that β-gal is a

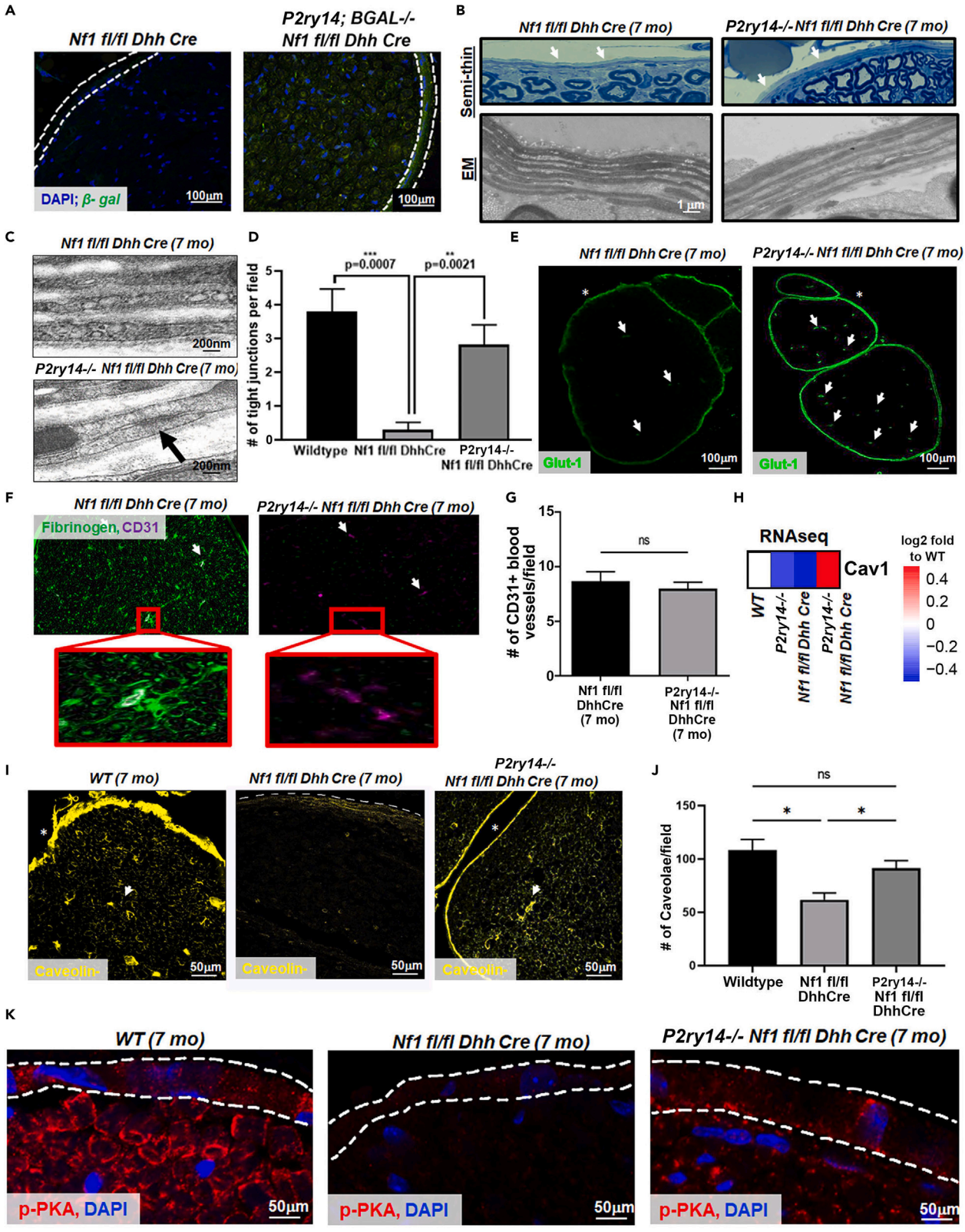
A
Nf1 fl/fl Dhh Cre
P2ry14; BGAL-/-
Nf1 fl/fl Dhh Cre
DAPI; β- gal
100µm
100µm
B
Nf1 fl/fl Dhh Cre (7 mo)
P2ry14-/-Nf1 fl/fl Dhh Cre (7 mo)
Semi-thin
EM
1 µm
C
Nf1 fl/fl Dhh Cre (7 mo)
200nm
P2ry14-/- Nf1 fl/fl Dhh Cre (7 mo)
200nm
D
p=0.0007
p=0.0021
# of tight junctions per field
Wildtype
Nf1 fl/fl DhhCre
P2ry14-/-
Nf1 fl/fl DhhCre
E
Nf1 fl/fl Dhh Cre (7 mo)
P2ry14-/- Nf1 fl/fl Dhh Cre (7 mo)
Glut-1
100µm
Glut-1
100µm
F
Nf1 fl/fl Dhh Cre (7 mo)
P2ry14-/- Nf1 fl/fl Dhh Cre (7 mo)
Fibrinogen, CD31
G
ns
# of CD31+ blood vessels/field
Nf1 fl/fl DhhCre (7 mo)
P2ry14-/- Nf1 fl/fl DhhCre (7 mo)
H
RNAseq
Cav1
log2 fold to WT
0.4
0.2
0
−0.2
−0.4
WT
P2ry14-/- Nf1 fl/fl Dhh Cre
P2ry14-/- Nf1 fl/fl Dhh Cre
I
WT (7 mo)
Nf1 fl/fl Dhh Cre (7 mo)
P2ry14-/- Nf1 fl/fl Dhh Cre (7 mo)
Caveolin-
50µm
Caveolin-
50µm
Caveolin-
50µm
J
ns
# of Caveolae/field
Wildtype
Nf1 fl/fl DhhCre
P2ry14-/- Nf1 fl/fl DhhCre
K
WT (7 mo)
Nf1 fl/fl Dhh Cre (7 mo)
P2ry14-/- Nf1 fl/fl Dhh Cre (7 mo)
p-PKA, DAPI
50µm
p-PKA, DAPI
50µm
p-PKA, DAPI
50µm

Figure 4. *P2ry14* knockout in Nf1fl/fl; Dhh+ mice restores BNB morphology, reduces fibrinogen deposition and increases Cav1 expression

(A) β-galactosidase immunofluorescent staining of 7-month-old *Nf1fl/fl;Dhh+* and *P2ry14*$^{-/-}$;*Nf1fl/fl;Dhh+* sciatic nerve shows P2RY14 knockdown (dotted lines denote the perineurium; *Nf1 fl/fl DhhCre* $n = 3$; *P2ry14*$^{-/-}$;*Nf1fl/flDhh+* $n = 3$).

(B) Nerve semi-thin sections and electron micrographs of 7-month *Nf1fl/fl;Dhh+* and *P2RY14*$^{-/-}$;*Nf1fl/fl;Dhh+* saphenous nerve showing perineurium structure (arrows denote perineurium).

(C) Electron micrograph showing TJs (arrow) in 7-month *Nf1fl/fl;Dhh+* and *P2RY14*$^{-/-}$;*Nf1fl/fl;Dhh+* saphenous nerve (*Nf1 fl/fl Dhh+* $n = 3$; *P2RY14 Nf1 fl/fl Dhh+* $n = 3$).

(D) Quantification of TJs per field of view (**$p = 0.0021$; ***$p = 0.0007$; one-way Anova) (*WT* $n = 3$; *Nf1 fl/fl Dhh+* $n = 3$; *P2ry14*$^{-/-}$;*Nf1fl/fl;Dhh+* $n = 3$).

(E) Anti-Glut1 immunofluorescent staining of 7-month *Nf1fl/fl;Dhh+* and *P2ry14*$^{-/-}$;*Nf1fl/fl;Dhh* sciatic nerve (arrows indicate Glut1+ endoneurial capillaries). (*Nf1 fl/fl Dhh+* $n = 3$; *P2ry14*$^{-/-}$;*Nf1fl/fl;Dhh+* $n = 3$).

(F) Anti fibrin/fibrinogen and anti-CD31 staining in 7-month *Nf1fl/fl;Dhh+* and *P2ry14*$^{-/-}$;*Nf1fl/fl;Dhh* sciatic nerve. Arrows point to CD31^{+} endoneurial capillaries, some of which are shown at increased magnification below boxed regions of the images (*Nf1 fl/fl Dhh+* $n = 3$; *P2ry14*$^{-/-}$;*Nf1fl/fl;Dhh* $n = 3$).

(G) Quantification of CD31^{+} endoneurial vessels in 7-month *Nf1fl/fl;Dhh+* and *P2ry14*$^{-/-}$;*Nf1fl/fl;Dhh* sciatic nerve (p = n.s.; un-paired t-test) (*Nf1 fl/fl Dhh+* $n = 3$; *P2ry14*$^{-/-}$;*Nf1fl/fl;Dhh* $n = 3$).

(H) RNAseq showing *Cav1* expression in nerve from 4-month-old *WT*, *P2ry14*$^{-/-}$, *Nf1fl/fl;Dhh+* and *P2ry14*$^{-/-}$;*Nf1fl/fl;Dhh+* sciatic nerve normalized to control wild-type mice. (*WT* $n = 3$, *P2ry14*$^{-/-}$ $n = 3$, *Nf1fl/fl;Dhh+* $n = 3$ and *P2ty14*$^{-/-}$;*Nf1fl/fl;Dhh+* $n = 3$).

(I) Anti-Caveolin immunofluorescent staining within 7-month *WT* and *Nf1fl/fl;Dhh+* sciatic nerve shows that in *WT* nerves, *Cav-1* expression is increased and localized to both the perineurium and the endoneurium. *Cav-1* expression is reduced in *Nf1 fl/flDhh+* sciatic nerve and rescued by genetic deletion of P2ry14. (*WT* $n = 3$, *Nf1fl/fl;Dhh+* $n = 3$ and *P2ry14*$^{-/-}$;*Nf1fl/fl;Dhh+* $n = 3$).

(J) Quantification of caveolae per field of view at the EM level in 7-month saphenous nerves (p = n.s. One-way Anova) (*WT* $n = 3$; *Nf1fl/fl;Dhh+* $n = 3$; *P2ry14*$^{-/-}$; *Nf1 fl/fl Dhh+* $n = 3$).

(K) anti-pPKA substrate immunofluorescent staining in 7-month *WT* and *Nf1fl/fl;Dhh+* sciatic nerve shows that in *WT* nerves, pPKA expression is localized to the perineurium (between dotted lines) as well as the endoneurium. Staining is reduced in *Nf1fl/fl;Dhh+* perineurium and endoneurium and rescued by genetic deletion of P2RY14. (*WT* $n = 3$; *Nf1fl/fl;Dhh+* $n = 3$; *P2ry14*$^{-/-}$;*Nf1fl/fl;Dhh+* $n = 3$). All stats Student's t test (Unpaired t-test) in all panels, n = numbers of individuals.

surrogate marker of *P2ry14* gene expression.[53] Beta-galactosidase staining was detected largely in the endoneurium in SCs, as shown previously.[39] In addition, close analysis showed that staining was also detectable in perineurial cells (between dotted lines) (Figure 4A). In saphenous nerve semi-thin sections, and in electron micrographs, *P2ry14*$^{-/-}$;*Nf1fl/fl;Dhh+* nerves showed similar morphology to that of *WT* nerves, with a well-organized perineurium morphology (Figure 4B). Strikingly, the number of TJs per field of view (Figures 4C and 4D), GLUT1 immunoreactivity (Figure 4E), and fibrinogen deposition (Figure 4F) were rescued in *P2ry14*$^{-/-}$;*Nf1fl/fl;Dhh+* nerves. No difference was observed in the number of CD31^{+} endoneurial vessels between cohorts (Figures 4F and 4G).

To determine if P2RY14 affects perineurial cell transcytosis in the context of *Nf1* loss in SCs we performed RNA sequencing of cDNA prepared from 4-month sciatic nerves. Low *Cav-1* transcript levels in *Nf1fl/fl;Dhh+* nerves were increased in the double mutant nerves (Figure 4H). We also stained sciatic nerve sections from 7-month-old mice with anti-caveolin. Double mutant *P2ry14*$^{-/-}$;*Nf1fl/fl;Dhh+* mice showed a partial increase caveolin expression in both the perineurium and the endoneurial space, with levels approaching those of WT nerve (Figure 4I). We measured perineurial cell caveolae numbers at the electron micrograph level in the saphenous nerve, and verified a partial rescue of caveolae (Figure 4J). Correlating with known effects of P2RY14 signaling, *p*-PKA substrate staining (Figure 4K) increased in both the perineurium and the endoneurium in the *P2ry14*$^{-/-}$;*Nf1fl/fl;Dhh+* nerve. Thus, in the *Nf1fl/fl;Dhh+* neurofibroma mouse model, genetic deletion of purinergic receptor P2RY14 improves nerve perineurium morphology, partially rescues fibrinogen deposition, rescues TJs, and partially rescues *Cav-1* expression, phenotypes which correlate with BNB permeability.

Pharmacological inhibition of P2RY14 restores nerve *p*-PKA and Cav1 expression

We tested if short-term pharmacological inhibition of the P2RY14 receptor is sufficient to restore the BNB in *Nf1fl/fl;Dhh+* mice. We treated 4-month-old *Nf1fl/fl;Dhh+* mice with the P2RY14 inhibitor PPTN (4-[4-(4-piperidinyl)phenyl]-7-[4-(trifluoromethyl)phenyl]-2-naphthalenecarboxylic acid) hydrochloride[54] for 14 days (Figure 5A). Confirming treatment efficacy, *p*-PKA substrate staining increased to near *WT* levels in PPTN treated mice, in both the perineurium (dotted lines) and, as previously described, the endoneurium[39] (Figure 5B). Fibrinogen deposition did not noticeably change after treatment, likely due to the brevity of PPTN treatment (Figure 5C). Notably, caveolin immunoreactivity increased in the perineurium after this short-term treatment with the P2RY14 inhibitor PPTN (Figure 5D). Together, the data are consistent with the hypothesis that P2RY14 regulates PKA and *Cav-1* expression in the BNB in the absence of *Nf1* in SCs. These data suggest a previously unappreciated high degree of plasticity in the BNB regulated by purinergic signaling.

DISCUSSION

The mechanisms that control the maintenance of the BNB and that regulate nerve homeostasis remain incompletely understood.[3,4,7,20,55,56] Understanding BNB regulation may identify therapeutic targets to regenerate the damaged or compromised BNB found in neuropathies and in nerve tumors. Our findings offer a clear demonstration that BNB integrity is regulated by SCs in a non-cell autonomous manner. We found that *Nf1* mutant SCs, known to increase their production and release of growth factors,[57,58] impacted the surrounding perineurial and endothelial cells, leading to a "leaky" BNB. Supporting this idea, increasing RTK expression/signaling together with loss of *Cav1* promoted barrier dysfunction and nerve tumors. Reduced *Cav1* in PNF is consistent with the idea that *CAV1* functions as a tumor-suppressor in human colon cancer, prostate cancer, and sarcomas.[59–61] We also showed that cross-talk between SC Nf1-Ras signaling and GPCR signaling controls the

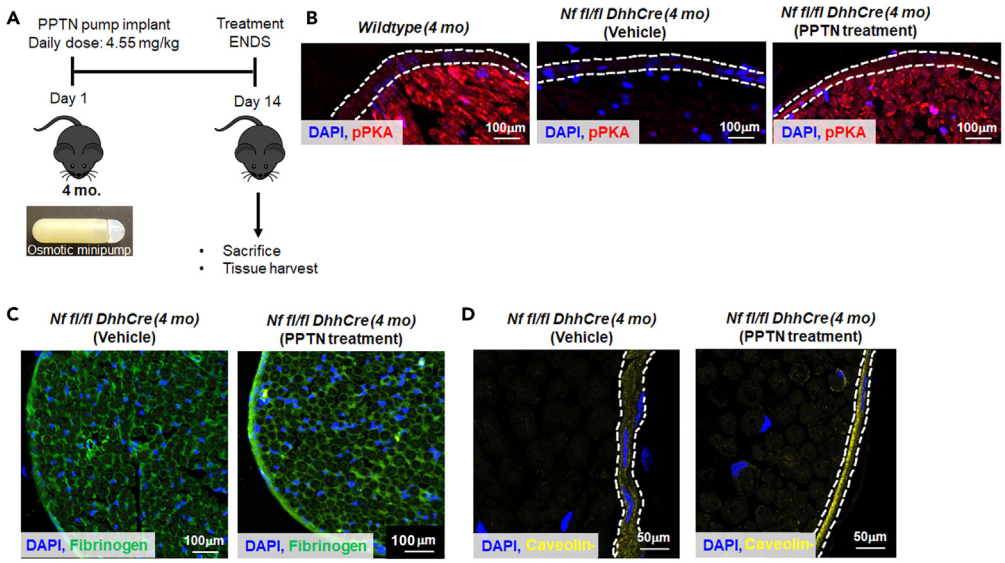

Figure 5. Pharmacological inhibition of P2RY14 restores nerve p-PKA and *Cav1* expression

(A) Illustration of experimental design to treat mice with the P2RY14 inhibitor (PPTN) drug via osmotic minipump delivery to 4-month *WT* and *Nf1fl/fl;Dhh+* mice.

(B) Anti-*p*-PKA-substrate immunofluorescent sciatic nerve staining of 4-month *WT*, *Nf1fl/fl;Dhh+* (Vehicle) and *Nf1fl/fl;Dhh+* (PPTN treated) mice showing that *p*-PKA expression is rescued to *WT* levels in PPTN treated mice.

(C) Anti-fibrinogen immunofluorescent staining with antibody is not changed with treatment.

(D) anti-caveolin immunofluorescent staining shows rescue by PPTN treatment in double mutants. (*WT* $n = 3$, *Nf1fl/fl;Dhh+* (Vehicle) $n = 3$, and *Nf1fl/fl;Dhh+* (PPTN treated) $n = 3$).

BNB. Thus, after *Nf1* loss, P2RY14 perturbs barrier function, at least in part through reducing *Cav1*. Understanding these pathways should aid in the re-establishment of the BNB to prevent nerve tumor progression and possibly to alleviate the debilitating effects of neuropathies.

Many PNFs are inoperable and enlargement of PNFs can cause profound nerve damage and/or compress nearby vital organs.[62] Whether a compromised BNB contributes to neurofibroma growth remains an important unanswered question. Consistent with the idea that leak is permissive for NF1-driven tumors, PNFs frequently form near peripheral ganglia and dermal neurofibromas form at cutaneous nerve endings; both locations show increased leak as compared to nerve trunks.[4] To address this, we used the *Nf1fl/fl;Dhh+* mouse model. At 4-month of age, when a few tumors begin to appear at cervical levels in this model,[16,63] leak into the endoneurium becomes detectable in lumbar nerves. Further, disruption of the BNB occurs not only in PNF, but also in the nerve of *Nf1* mutant mice, where tumors do not form. Therefore, BNB disruption is not sufficient to drive tumor formation. However, BNB disruption and tumor formation occur in tandem so that the timing of phenotypes does not suggest that one causes the other.

We also found that signaling via P2RY14 is a critical mediator of BNB integrity in NF1. The production of factors by mammalian SC affecting the BNB is exemplified by SC production of desert hedgehog, which contributes to formation of the perineurium during murine development through interaction with the GPCR Patched.[64] In the fly, the Amnesiac (*amn*) neuropeptide binds to and activates GPCR signaling.[65] *Amn* loss in fly's nerves thickened the perineurial glia layer, an effect potentiated by loss of *Nf1*.[66] Like our data, this suggests cross-talk between Ras and GPCR in interaction between endoneurial SC and surrounding perineurial cells. Modulation of additional GPCR might, like P2RY14, similarly affect the BNB. IP10/CXCL10, a chemokine ligand for the GPCR CXCR3, is upregulated in *Nf1* mutant SCs,[16] and is a candidate factor for affecting the BNB, as increases in IP10/CXCL10 correlate with dysfunction of the BNB in some peripheral neuropathies.[67] However, whether the rescue of all the effects we describe on the BNB are caused by P2RY14 in *Nf1* mutant SCs is unclear. P2ry14 expression is highest in nerve SCs, but P2RY14 is also expressed in perineurial and endothelial cells. The development of P2RY14 conditional knockouts should determine if changes in BNB permeability are mediated by one or a combination of cell types.[68] Even if not SC specific, current studies are consistent with the idea that the BNB has a high-level of plasticity, as modulation of P2RY14 signaling, via genetic deletion or pharmacological inhibition in our *Nf1* loss-driven PNF mouse model, led to partial normalization of BNB disruption phenotypes. The availability of a therapeutic P2RY14 inhibitor compound with improved properties should enable the study of the effects on PNF growth and clarify the long-term effects of P2RY14 inhibition on the BNB.

How caveolae and TJs are remodeled during BNB disruption and re-establishment in NF1 remains unclear. The BNB is maintained by TJs between adjacent endothelial cells in the endoneurium, and between adjacent perineurial cells. Increasing transcytosis following nerve injury or acutely elevating Raf in Schwann cells also promotes leak in the BNB.[3] Our finding of reduced *Cav1*/caveolae correlating with a leaky BNB is surprising given these results. However, loss of Cav1 also reduces junctional localization of tight junction proteins, accompanied by increased paracellular permeability through adjacent endothelial cells, causing diminished expression and altered subcellular distribution of major junctional proteins. Indeed, we visualized mislocalized ZO-1 in the *Nf1 fl/fl Dhh+* perineurium. In sum, primary effects on either TJs or caveolae may contribute the leak observed; the interplay between TJs and caveolae in barrier function is likely to be important.

The mechanism(s) underlying *Cav1* mRNA and caveolin protein downregulation in the NF1 nerve are not clear. The NF1 protein neurofibromin and Cav1 proteins may interact,[69] so that in SCs lacking *Nf1*, Cav1 protein might be destabilized or mislocalized. Also, *Nf1* loss in SCs elevates RAS-MAPK signaling. Reducing *Cav1* mRNA in SCs likely occurs downstream of Ras-GTP, as Ras-MAPK-driven lowering of Cav1 increases Ras-MAPK signaling in other cell types.[70] In NF1, such a feedforward loop is predicted to enhance BNB perturbation. In support of this idea, increasing RAS-MAPK signaling in SCs by EGFR expression failed to significantly perturb the BNB, yet reducing *Cav1* in the context of enhanced EGFR expression in SC (CNPase-EGFR) did perturb the BNB. We suggest that elevated RAS-MAPK signaling resulting from reduced *Cav1* expression results in barrier disruption.

Given that pharmacological blockade of the P2RY14 receptor improves NF1-dependent disruption of the BNB, therapies targeting P2RY14 and/or its downstream effector signaling may be useful in treating NF1 patients, and more globally be useful in those afflicted with debilitating neuropathies.

Limitations of the study

It remains unclear whether changes in BNB permeability are mediated by P2RY14 loss in one or a combination of cell types. Cell type-specific conditional knockouts will be needed to test whether effects are in Schwann cells, perineurial cells, or both cell types. Additionally, the P2RY14 inhibitor we used to rescue BNB permeability is a tool compound with limited bioavailability. A P2RY14 inhibitor compound with improved properties would allow definition of potential long-term effects of P2RY14 inhibition on the BNB, and of potential effects of P2RY14 blockade on human neurofibromas.

STAR★METHODS

Detailed methods are provided in the online version of this paper and include the following:

- KEY RESOURCES TABLE
- RESOURCE AVAILABILITY
  - Lead contact
  - Materials availability
  - Data and code availability
- EXPERIMENTAL MODEL AND STUDY PARTICIPANT DETAILS
- METHOD DETAILS
  - Immunostaining
  - IgA and alpha 2 Macroglobulin immunohistochemistry
  - Electron microscopy
  - CNPAse-hEGFR Cav1 mice protocol
  - RNA sequencing
  - Osmotic pump drug study
- QUANTIFICATION AND STATISTICAL ANALYSIS

SUPPLEMENTAL INFORMATION

Supplemental information can be found online at https://doi.org/10.1016/j.isci.2024.110294.

ACKNOWLEDGMENTS

We thank Takeda Cambridge Limited and Dr. Johannes Grosse for providing the P2YR14 knock-in mouse. We thank Sylvie Breton, PhD and Maria Agustina Battistone, PhD from Harvard Medical School and Massachusetts General Hospital for guidance on the P2RY14 antagonist osmotic minipump drug study. We thank Noah Reitz for helping with tissue immunostaining, and Jay Pundavela for the diagram in Figure 1A, created with Biorender.com. The graphical abstract for this paper was also created with BioRender.com. J.P-C. was supported by NIH-T32-NS007453 and a Children's Tumor Foundation Young Investigator Award. This work was supported by grants NIH-R01-NS28840, NIH-R37-NS083580 to N.R and NIH-RO1-NS115438 to N.R. and D.A.L.

AUTHOR CONTRIBUTIONS

Conceptualization: N.R. and D.A.L. methodology: J.P-C., T.A.R., K.E.C., and E.P.R. validation: J.P-C. and E.P.R. formal analysis: J.P-C., N.R., and E.P.R. investigation: J.P-C. and E.P.R. resources: N.R. and D.A.L. writing—original draft: J.P-C. and N.R.; writing—review & editing: T.N.P. and D.A.L.; visualization: J.P-C., E.P.R., D.A.L., and N.R.; supervision: N.R. and D.A.L., funding acquisition: N.R., D.A.L., and J.P-C.

DECLARATION OF INTERESTS

Some research in the N.R. lab is funded by Revolution Meidicines and Boehringer Ingelheim, unrelated to this study. D.A.L. is the co-founder and co-owner of NeoClone Biotechnologies, Inc., Discovery Genomics, Inc. (recently acquired by Immusoft, Inc.), B-MoGen Biotechnologies, Inc. (recently acquired by Bio-Techne Corporation), and Luminary Therapeutics, Inc. D.A.L. holds equity in, serves as a Senior Scientific Advisor

for and Board of Director member for Recombinetics, a genome editing company. The business of all these companies is unrelated to the contents of this manuscript. D.A.L. consults for Styx Therapeutics, Inc. and Genentech, Inc., which is funding some of his research.

Received: June 10, 2022
Revised: December 17, 2023
Accepted: June 14, 2024
Published: June 17, 2024

REFERENCES

1. Rechthand, E., and Rapoport, S.I. (1987). Regulation of the microenvironment of peripheral nerve: role of the blood-nerve barrier. Prog. Neurobiol. *28*, 303–343.
2. Ubogu, E.E. (2020). Biology of the human blood-nerve barrier in health and disease. Exp. Neurol. *328*, 113272.
3. Malong, L., Napoli, I., Casal, G., White, I.J., Stierli, S., Vaughan, A., Cattin, A.L., Burden, J.J., Hng, K.I., Bossio, A., et al. (2023). Characterization of the structure and control of the blood-nerve barrier identifies avenues for therapeutic delivery. Dev. Cell *58*, 174–191.e8.
4. Mizisin, A.P., and Weerasuriya, A. (2011). Homeostatic regulation of the endoneurial microenvironment during development, aging and in response to trauma, disease and toxic insult. Acta Neuropathol. *121*, 291–312.
5. Olsson, Y. (1990). Microenvironment of the peripheral nervous system under normal and pathological conditions. Crit. Rev. Neurobiol. *5*, 265–311.
6. Parton, R.G. (2018). Caveolae: Structure, Function, and Relationship to Disease. Annu. Rev. Cell Dev. Biol. *34*, 111–136.
7. Thomas, P.K. (1963). The connective tissue of peripheral nerve: an electron microscope study. J. Anat. *97*, 35–44.
8. Cattin, A.L., Burden, J.J., Van Emmenis, L., Mackenzie, F.E., Hoving, J.J.A., Garcia Calavia, N., Guo, Y., McLaughlin, M., Rosenberg, L.H., Quereda, V., et al. (2015). Macrophage-Induced Blood Vessels Guide Schwann Cell-Mediated Regeneration of Peripheral Nerves. Cell *162*, 1127–1139.
9. de la Motte, D.J., Hall, S.M., and Allt, G. (1975). A study of the perineurium in peripheral nerve pathology. Acta Neuropathol. *33*, 257–270. https://doi.org/10.1007/BF00688398.
10. Reinhold, A.K., and Rittner, H.L. (2020). Characteristics of the nerve barrier and the blood dorsal root ganglion barrier in health and disease. Exp. Neurol. *327*, 113244.
11. Agaimy, A. (2014). Microscopic intraneural perineurial cell proliferations in patients with neurofibromatosis type 1. Ann. Diagn. Pathol. *18*, 95–98.
12. Schober, R., Vogeley, K.T., Urich, H., Hölzle, E., and Wechsler, W. (1992). Vascular permeability changes in tumours of the peripheral nervous system. Virchows Arch. A Pathol. Anat. Histopathol. *420*, 59–64.
13. Bergoug, M., Doudeau, M., Godin, F., Mosrin, C., Vallée, B., and Bénédetti, H. (2020). Neurofibromin Structure, Functions and Regulation. Cells *9*, 2365.
14. Hirose, T., Tani, T., Shimada, T., Ishizawa, K., Shimada, S., and Sano, T. (2003). Immunohistochemical demonstration of EMA/Glut1-positive perineurial cells and CD34-positive fibroblastic cells in peripheral nerve sheath tumors. Mod. Pathol. *16*, 293–298.
15. Zamecnik, M., and Michal, M. (2001). Perineurial cell differentiation in neurofibromas. Report of eight cases including a case with composite perineurioma-neurofibroma features. Pathol. Res. Pract. *197*, 537–544.
16. Fletcher, J.S., Wu, J., Jessen, W.J., Pundavela, J., Miller, J.A., Dombi, E., Kim, M.O., Rizvi, T.A., Chetal, K., Salomonis, N., and Ratner, N. (2019). Cxcr3-expressing leukocytes are necessary for neurofibroma formation in mice. JCI Insight *4*, e98601.
17. Prada, C.E., Jousma, E., Rizvi, T.A., Wu, J., Dunn, R.S., Mayes, D.A., Cancelas, J.A., Dombi, E., Kim, M.O., West, B.L., et al. (2013). Neurofibroma-associated macrophages play roles in tumor growth and response to pharmacological inhibition. Acta Neuropathol. *125*, 159–168.
18. Sun, Y., Hu, G., Zhang, X., and Minshall, R.D. (2009). Phosphorylation of caveolin-1 regulates oxidant-induced pulmonary vascular permeability via paracellular and transcellular pathways. Circ. Res. *105*, 676–685.
19. Gu, Y., Zheng, G., Xu, M., Li, Y., Chen, X., Zhu, W., Tong, Y., Chung, S.K., Liu, K.J., and Shen, J. (2012). Caveolin-1 regulates nitric oxide-mediated matrix metalloproteinases activity and blood-brain barrier permeability in focal cerebral ischemia and reperfusion injury. J. Neurochem. *120*, 147–156.
20. Oldfors, A., and Johansson, B.R. (1979). Barriers and transport properties of the perineurium. An ultrastructural study with 125I-labeled albuminin and horseradish peroxidase in normal and protein-deprived rats. Acta Neuropathol. *47*, 139–143.
21. Couet, J., Sargiacomo, M., and Lisanti, M.P. (1997). Interaction of a receptor tyrosine kinase, EGF-R, with caveolins. Caveolin binding negatively regulates tyrosine and serine/threonine kinase activities. J. Biol. Chem. *272*, 30429–30438.
22. Huang, C., Hepler, J.R., Chen, L.T., Gilman, A.G., Anderson, R.G., and Mumby, S.M. (1997). Organization of G proteins and adenylyl cyclase at the plasma membrane. Mol. Biol. Cell *8*, 2365–2378.
23. Li, S., Couet, J., and Lisanti, M.P. (1996). Src tyrosine kinases, Galpha subunits, and H-Ras share a common membrane-anchored scaffolding protein, caveolin. Caveolin binding negatively regulates the auto-activation of Src tyrosine kinases. J. Biol. Chem. *271*, 29182–29190.
24. Rybin, V.O., Xu, X., Lisanti, M.P., and Steinberg, S.F. (2000). Differential targeting of beta -adrenergic receptor subtypes and adenylyl cyclase to cardiomyocyte caveolae. A mechanism to functionally regulate the cAMP signaling pathway. J. Biol. Chem. *275*, 41447–41457.
25. Kuo, A., Lee, M.Y., Yang, K., Gross, R.W., and Sessa, W.C. (2018). Caveolin-1 regulates lipid droplet metabolism in endothelial cells via autocrine prostacyclin-stimulated, cAMP-mediated lipolysis. J. Biol. Chem. *293*, 973–983.
26. Razani, B., and Lisanti, M.P. (2001). Two distinct caveolin-1 domains mediate the functional interaction of caveolin-1 with protein kinase A. Am. J. Physiol. Cell Physiol. *281*, C1241–C1250.
27. Hnasko, R., and Lisanti, M.P. (2003). The biology of caveolae: lessons from caveolin knockout mice and implications for human disease. Mol. Interv. *3*, 445–464.
28. Savio, L.E.B., de Andrade Mello, P., Santos, S.A.C.S., de Sousa, J.C., Oliveira, S.D.S., Minshall, R.D., Kurtenbach, E., Wu, Y., Longhi, M.S., Robson, S.C., and Coutinho-Silva, R. (2020). P2X7 receptor activation increases expression of caveolin-1 and formation of macrophage lipid rafts, thereby boosting CD39 activity. J. Cell Sci. *133*, jcs237560. https://doi.org/10.1242/jcs.237560.
29. Chen, X., Qian, S., Hoggatt, A., Tang, H., Hacker, T.A., Obukhov, A.G., Herring, P.B., and Seye, C.I. (2017). Endothelial Cell-Specific Deletion of P2Y2 Receptor Promotes Plaque Stability in Atherosclerosis-Susceptible ApoE-Null Mice. Arterioscler. Thromb. Vasc. Biol. *37*, 75–83.
30. Hechler, B., Freund, M., Ravanat, C., Magnenat, S., Cazenave, J.P., and Gachet, C. (2008). Reduced atherosclerotic lesions in P2Y1/apolipoprotein E double-knockout mice: the contribution of non-hematopoietic-derived P2Y1 receptors. Circulation *118*, 754–763.
31. Horckmans, M., Esfahani, H., Beauloye, C., Clouet, S., di Pietrantonio, L., Robaye, B., Balligand, J.L., Boeynaems, J.M., Dessy, C., and Communi, D. (2015). Loss of mouse P2Y4 nucleotide receptor protects against myocardial infarction through endothelin-1 downregulation. J. Immunol. *194*, 1874–1881.
32. Lou, N., Takano, T., Pei, Y., Xavier, A.L., Goldman, S.A., and Nedergaard, M. (2016). Purinergic receptor P2RY12-dependent microglial closure of the injured blood-brain barrier. Proc. Natl. Acad. Sci. USA *113*, 1074–1079.
33. Stachon, P., Peikert, A., Michel, N.A., Hergeth, S., Marchini, T., Wolf, D., Dufner, B., Hoppe, N., Ayata, C.K., Grimm, M., et al. (2014). "P2Y6 deficiency limits vascular inflammation and atherosclerosis in mice. Arterioscler. Thromb. Vasc. Biol. *34*, 2237–2245.
34. Talley Watts, L., Sprague, S., Zheng, W., Garling, R.J., Jimenez, D., Digicaylioglu, M., and Lechleiter, J. (2013). Purinergic 2Y1 receptor stimulation decreases cerebral edema and reactive gliosis in a traumatic brain injury model. J. Neurotrauma *30*, 55–66.
35. Harden, T.K., Sesma, J.I., Fricks, I.P., and Lazarowski, E.R. (2010). Signalling and pharmacological properties of the P2Y receptor. Acta Physiol. *199*, 149–160.

36. Carman, A.J., Mills, J.H., Krenz, A., Kim, D.G., and Bynoe, M.S. (2011). Adenosine receptor signaling modulates permeability of the blood-brain barrier. J. Neurosci. *31*, 13272–13280.
37. Mills, J.H., Thompson, L.F., Mueller, C., Waickman, A.T., Jalkanen, S., Niemela, J., Airas, L., and Bynoe, M.S. (2008). CD73 is required for efficient entry of lymphocytes into the central nervous system during experimental autoimmune encephalomyelitis. Proc. Natl. Acad. Sci. USA *105*, 9325–9330.
38. Carter, R.L., Fricks, I.P., Barrett, M.O., Burianek, L.E., Zhou, Y., Ko, H., Das, A., Jacobson, K.A., Lazarowski, E.R., and Harden, T.K. (2009). Quantification of Gi-mediated inhibition of adenylyl cyclase activity reveals that UDP is a potent agonist of the human P2Y14 receptor. Mol. Pharmacol. *76*, 1341–1348.
39. Patritti-Cram, J., Wu, J., Coover, R.A., Rizvi, T.A., Chaney, K.E., Ravindran, R., Cancelas, J.A., Spinner, R.J., and Ratner, N. (2022). P2RY14 cAMP signaling regulates Schwann cell precursor self-renewal, proliferation, and nerve tumor initiation in a mouse model of neurofibromatosis. Elife *11*, e73511.
40. Li, F., Li, W., Li, X., Li, F., Zhang, L., Wang, B., Huang, G., Guo, X., Wan, L., Liu, Y., et al. (2016). Geniposide attenuates inflammatory response by suppressing P2Y14 receptor and downstream ERK1/2 signaling pathway in oxygen and glucose deprivation-induced brain microvascular endothelial cells. J. Ethnopharmacol. *185*, 77–86.
41. Iwanaga, T., Takahashi-Iwanaga, H., Nio-Kobayashi, J., and Ebara, S. (2022). Structure and barrier functions of the perineurium and its relationship with associated sensory corpuscles: A review. Biomed. Res. *43*, 145–159.
42. Pina, A.R., Martinez, M.M., and de Almeida, O.P. (2015). Glut1, best immunohistochemical marker for perineurial cells. Head Neck Pathol *9*, 104–106.
43. Petersen, M.A., Ryu, J.K., and Akassoglou, K. (2018). Fibrinogen in neurological diseases: mechanisms, imaging and therapeutics. Nat. Rev. Neurosci. *19*, 283–301.
44. Li, X., Fetter, R., Schwabe, T., Jung, C., Liu, L., Steller, H., and Gaul, U. (2021). The cAMP effector PKA mediates Moody GPCR signaling in Drosophila blood-brain barrier formation and maturation. Elife *10*, e68275.
45. Cucullo, L., Marchi, N., Marroni, M., Fazio, V., Namura, S., and Janigro, D. (2003). Blood-brain barrier damage induces release of alpha2-macroglobulin. Mol. Cell. Proteomics *2*, 234–241. https://doi.org/10.1074/mcp.M200077-MCP200.
46. Hadden, R.D.M., Gregson, N.A., Gold, R., Smith, K.J., and Hughes, R.A.C. (2002). Accumulation of immunoglobulin across the 'blood-nerve barrier' in spinal roots in adoptive transfer experimental autoimmune neuritis. Neuropathol. Appl. Neurobiol. *28*, 489–497. https://doi.org/10.1046/j.1365-2990.2002.00421.x.
47. Wu, J., Williams, J.P., Rizvi, T.A., Kordich, J.J., Witte, D., Meijer, D., Stemmer-Rachamimov, A.O., Cancelas, J.A., and Ratner, N. (2008). Plexiform and dermal neurofibromas and pigmentation are caused by Nf1 loss in desert hedgehog-expressing cells. Cancer Cell *13*, 105–116.
48. Rahrmann, E.P., Watson, A.L., Keng, V.W., Choi, K., Moriarity, B.S., Beckmann, D.A., Wolf, N.K., Sarver, A., Collins, M.H., Moertel, C.L., et al. (2013). Forward genetic screen for malignant peripheral nerve sheath tumor formation identifies new genes and pathways driving tumorigenesis. Nat. Genet. *45*, 756–766.
49. Ling, B.C., Wu, J., Miller, S.J., Monk, K.R., Shamekh, R., Rizvi, T.A., Decourten-Myers, G., Vogel, K.S., DeClue, J.E., and Ratner, N. (2005). Role for the epidermal growth factor receptor in neurofibromatosis-related peripheral nerve tumorigenesis. Cancer Cell *7*, 65–75.
50. Galbiati, F., Volonte, D., Engelman, J.A., Watanabe, G., Burk, R., Pestell, R.G., and Lisanti, M.P. (1998). Targeted downregulation of caveolin-1 is sufficient to drive cell transformation and hyperactivate the p42/44 MAP kinase cascade. EMBO J. *17*, 6633–6648.
51. Wu, J., Liu, W., Williams, J.P., and Ratner, N. (2017). EGFR-Stat3 signalling in nerve glial cells modifies neurofibroma initiation. Oncogene *36*, 1669–1677.
52. Keng, V.W., Rahrmann, E.P., Watson, A.L., Tschida, B.R., Moertel, C.L., Jessen, W.J., Rizvi, T.A., Collins, M.H., Ratner, N., and Largaespada, D.A. (2012). PTEN and NF1 inactivation in Schwann cells produces a severe phenotype in the peripheral nervous system that promotes the development and malignant progression of peripheral nerve sheath tumors. Cancer Res. *72*, 3405–3413.
53. Meister, J., Le Duc, D., Ricken, A., Burkhardt, R., Thiery, J., Pfannkuche, H., Polte, T., Grosse, J., Schöneberg, T., and Schulz, A. (2014). The G protein-coupled receptor P2Y14 influences insulin release and smooth muscle function in mice. J. Biol. Chem. *289*, 23353–23366.
54. Robichaud, J., Fournier, J.F., Gagné, S., Gauthier, J.Y., Hamel, M., Han, Y., Hénault, M., Kargman, S., Levesque, J.F., Mamane, Y., et al. (2011). Applying the pro-drug approach to afford highly bioavailable antagonists of P2Y(14). Bioorg. Med. Chem. Lett. *21*, 4366–4368.
55. Burkel, W.E. (1967). The histological fine structure of perineurium. Anat. Rec. *158*, 177–189.
56. Gamble, H.J., and Eames, R.A. (1964). An Electron Microscope Study of the Connective Tissues of Human Peripheral Nerve. J. Anat. *98*, 655–663.
57. Choi, K., Komurov, K., Fletcher, J.S., Jousma, E., Cancelas, J.A., Wu, J., and Ratner, N. (2017). An inflammatory gene signature distinguishes neurofibroma Schwann cells and macrophages from cells in the normal peripheral nervous system. Sci. Rep. *7*, 43315.
58. Yang, F.-C., Ingram, D.A., Chen, S., Hingtgen, C.M., Ratner, N., Monk, K.R., Clegg, T., White, H., Mead, L., Wenning, M.J., et al. (2003). Neurofibromin-deficient Schwann cells secrete a potent migratory stimulus for Nf1+/- mast cells. J. Clin. Invest. *112*, 1851–1861. https://doi.org/10.1172/JCI19195.
59. Ayala, G., Morello, M., Frolov, A., You, S., Li, R., Rosati, F., Bartolucci, G., Danza, G., Adam, R.M., Thompson, T.C., et al. (2013). Loss of caveolin-1 in prostate cancer stroma correlates with reduced relapse-free survival and is functionally relevant to tumour progression. J. Pathol. *231*, 77–87.
60. Bender, F.C., Reymond, M.A., Bron, C., and Quest, A.F. (2000). Caveolin-1 levels are down-regulated in human colon tumors, and ectopic expression of caveolin-1 in colon carcinoma cell lines reduces cell tumorigenicity. Cancer Res. *60*, 5870–5878.
61. Wiechen, K., Sers, C., Agoulnik, A., Arlt, K., Dietel, M., Schlag, P.M., and Schneider, U. (2001). Down-regulation of caveolin-1, a candidate tumor suppressor gene, in sarcomas. Am. J. Pathol. *158*, 833–839.
62. Armstrong, A.E., Belzberg, A.J., Crawford, J.R., Hirbe, A.C., and Wang, Z.J. (2023). Treatment decisions and the use of MEK inhibitors for children with neurofibromatosis type 1-related plexiform neurofibromas. BMC Cancer *23*, 553.
63. Fletcher, J.S., Pundavela, J., and Ratner, N. (2020). After Nf1 loss in Schwann cells, inflammation drives neurofibroma formation. Neurooncol. Adv. *2*, i23–i32.
64. Parmantier, E., Lynn, B., Lawson, D., Turmaine, M., Namini, S.S., Chakrabarti, L., McMahon, A.P., Jessen, K.R., and Mirsky, R. (1999). Schwann cell-derived Desert hedgehog controls the development of peripheral nerve sheaths. Neuron *23*, 713–724.
65. Turrel, O., Rabah, Y., Plaçais, P.Y., Goguel, V., and Preat, T. (2020). Drosophila Middle-Term Memory: Amnesiac is Required for PKA Activation in the Mushroom Bodies, a Function Modulated by Neprilysin 1. J. Neurosci. *40*, 4219–4229.
66. Yager, J., Richards, S., Hekmat-Scafe, D.S., Hurd, D.D., Sundaresan, V., Caprette, D.R., Saxton, W.M., Carlson, J.R., and Stern, M. (2001). Control of Drosophila perineurial glial growth by interacting neurotransmitter-mediated signaling pathways. Proc. Natl. Acad. Sci. USA *98*, 10445–10450.
67. Shimizu, F., Oishi, M., Sawai, S., Beppu, M., Misawa, S., Matsui, N., Miyashiro, A., Maeda, T., Takeshita, Y., Nishihara, H., et al. (2019). Increased IP-10 production by blood-nerve barrier in multifocal acquired demyelinating sensory and motor neuropathy and multifocal motor neuropathy. J. Neurol. Neurosurg. Psychiatry *90*, 444–450.
68. Battistone, M.A., Mendelsohn, A.C., Spallanzani, R.G., Allegretti, A.S., Liberman, R.N., Sesma, J., Kalim, S., Wall, S.M., Bonventre, J.V., Lazarowski, E.R., et al. (2020). Proinflammatory P2Y14 receptor inhibition protects against ischemic acute kidney injury in mice. J. Clin. Invest. *130*, 3734–3749.
69. Boyanapalli, M., Lahoud, O.B., Messiaen, L., Kim, B., Anderle de Sylor, M.S., Duckett, S.J., Somara, S., and Mikol, D.D. (2006). Neurofibromin binds to caveolin-1 and regulates ras, FAK, and Akt. Biochem. Biophys. Res. Commun. *340*, 1200–1208.
70. Engelman, J.A., Zhang, X.L., Razani, B., Pestell, R.G., and Lisanti, M.P. (1999). p42/44 MAP kinase-dependent and -independent signaling pathways regulate caveolin-1 gene expression. Activation of Ras-MAP kinase and protein kinase a signaling cascades transcriptionally down-regulates caveolin-1 promoter activity. J. Biol. Chem. *274*, 32333–32341.
71. Edgar, R., Domrachev, M., and Lash, A.E. (2002). Gene Expression Omnibus: NCBI gene expression and hybridization array data repository. Nucleic Acids Res. *30*, 207–210.

STAR★METHODS

KEY RESOURCES TABLE

REAGENT or RESOURCE	SOURCE	IDENTIFIER
Antibodies		
Anti-Glut1 antibody	Abcam	Cat#ab115730; RRID: AB_10903230
Anti-Fibrin(ogen)	Agilent DAKO	Cat#: A008002-2; RRID: AB_2894406
Anti-CD#!	BD Biosciences	Cat#: 553370; RRID: AB_394816
Anti-pPKA substrate	Cell Signaling	Cat#: 9621S; RRID: AB_330304
Anti-Cav1	Cell Signaling	Cat#:3238S; RRID: AB_2072166
Anti-CD45	Novus Biologicals	Cat# 100-77417; RRID: AB_1724173
Anti-β-galactosidase	Thermo Fisher	Cat#: A-11132; RRID: AB_221539
Anti-Iba-1	Wako Chemicals	Cat#: 019-19741; RRID: AB_839504
Anti-Claudin-5	ThermoFisher Scientific	Cat# 341600; RRID: AB_2533157
Anti-ZO-1	ThermoFisher Scientific	Cat#: 402200; RRID: AB_431613
Anti-IgA	Cell Signaling	Cat # 50384
Anti-alpha 2 macroglobulin	Cell Signaling	Cat # 71610
Biological samples		
Human nerve	Cincinnati Children's Hospital	This paper.
Human plexiform neurofibroma tumors	Cincinnati Children's Hospital	This paper.
Chemicals, peptides, and recombinant proteins		
P2RY14 inhibitor (PPTN-HCl:4-[4-(4-Piperidinyl]-7-[4-(trifluoromethyl)phenyl]-2-naphthalenecarboxyliv acid hydrochloride)	TOCRIS	Cat #: 4862
Deposited data		
mouse RNA-Seq data	NCBI's Gene Expression Omnibus (Edgar, Domrachev, & Lash, 2002)	GEO Accession #189189
Mouse single cell RNAseq	NCBI's Gene Expression Omnibus (Edgar, Domrachev, & Lash, 2002)	GEO Accession #189189
Single cell RNA-Seq	NCBI's Gene Expression Omnibus (Edgar, Domrachev, & Lash, 2002)	GEO Accession #181985
Human microarray data	NCBI's Gene Expression Omnibus (Edgar, Domrachev, & Lash, 2002)	GEO Accession #: GSE14038
Experimental models: Organisms/strains		
Mouse: C57Bl/6 mice	The Jackson Laboratory	Strain #: 000664
Mouse: *Nf1fl/fl; Dhh+*	Cincinnati Children's Hospital and Medical Center	Wu et al., 2008
Mouse: *P2ry14+/-;Nf1fl/fl;Dhh+*	Cincinnati Children's Hospital and Medical Center	Patritti-Cram et al., 2022
Mouse: *P2ry14-/-;Nf1fl/fl; Dhh+*	Cincinnati Children's Hospital and Medical Center	Patritti-Cram et al., 2022
Mouse: *Cav1+/-*	University of Minnesota	Ling et al., 2005
Mouse: *CNPase-hEGFR*	University of Minnesota	Ling et al., 2005
Mouse: *Cav1+/-,CNPase-hEGF*	University of Minnesota	Ling et al., 2005
Software and algorithms		
ImageJ	Schneider et al.	https://imagej.nih.gov/ij/

RESOURCE AVAILABILITY

Lead contact

Further information and requests for resources and reagents should be directed to and will be fulfilled by the lead contact, Nancy Ratner, PhD (nancy.ratner@cchmc.org).

Materials availability

This study did not generate new unique reagents.

Data and code availability

- The mouse RNA-Seq and single cell RNAseq data generated for this publication have been deposited in NCBI's Gene Expression Omnibus[71] GEO Accession #189189 and are publicly available as of the date of publication. Single cell RNA-Seq data is available at GEO Accession #181985 and are publicly available as of the date of publication. Human microarray data is available at GEO Accession # GSE14038 and are publicly available as of the date of publication.
- This paper does not report original code.
- Any additional information required to reanalyze the data reported in this paper is available from the lead contact upon request.

EXPERIMENTAL MODEL AND STUDY PARTICIPANT DETAILS

We housed mice in a temperature and humidity-controlled vivarium on a 12hr dark-light cycle with free access to food and water. The animal care and use committee of Cincinnati Children's Hospital Medical Center approved all animal use. Wild type C57Bl/6 mice were from Jackson Laboratory and were used at 4 and 7 months of age. The Nf1fl/fl; Dhh+ mouse line has been described previously by Patritti et al.[47] WT C57Bl/6 mice were from Jackson Laboratory and were used at 4 and 7 months of age. The $Nf1^{fl/fl}$;DhhCre mouse line has been described previously by Wu et al., 2008. We bred $P2ry14^{-/-}$ male mice (Meister et al., 2014; Takeda Cambridge Limited) with $Nf1^{fl/fl}$ female mice to obtain the F1 generation $P2ry14^{+/-}$;$Nf1^{fl/+}$; then, we bred the F1 mice with $Nf1^{fl/fl}$;Dhh^{Cre} male mice to obtain $P2ry14^{+/-}$;$Nf1^{fl/+}$;Dhh^{Cre}. Then, we bred $P2ry14^{+/-}$;$Nf1^{fl/+}$;Dhh^{Cre} (males) with $P2ry14^{+/-}$;$Nf1^{fl/+}$; Dhh^{Cre} (females) to obtain $P2ry14^{+/-}$; $Nf1^{fl/fl}$;$Dhh^{Cre}$and P2ry14;$Nf1^{fl/fl}$;Dhh^{Cre}.[39] Genotyping of mice was carried out by PCR with the following primers: β-galactosidase sense (5′-AGAAGGCACATGGCTGAATATCGA-3′), forward (5′-AGCTGCCGGACGAAGGAGACCCTGCTC-3′), and reverse (5′-GGTTTTGGAAACCTCTAGGTCATTCTG-3′) in two separate PCRs; forward/reverse to amplify WT allele (180 bp) and β-galactosidase sense/reverse to amplify KO allele (400 bp). The PCR conditions were 95°C for 3 min followed by 35 cycles with 95°C for 45 s, 60°C for 30 s, and 72°C for 1 min and a final amplification step of 72°C for 10 min.[53] *Cnp-hEGFR* mice were genotyped by amplyfing $Egfr^{wa-2}$ a 170 bp region (primers: 5′-CCCAGAAAGGGATATGCG-3′ and 5′-GCAACCGTAGGGCATGAG-3′) and digesting with FokI to produce an uncut 170 bp or cut 75 and 95 bp fragments diagnostic for wild-type (wt) Egfr and $Egfr^{wa2}$ alleles, respectively, as reported.[49] The cross of CNP-EGFR mice to *Cav1-/-* mice was approved at by the University of Minnesota animal care and use committee. In all experiments, littermates were used for controls. Mice of both sexes (male and female) were used for all experiments in equal numbers. The animal care and use committee of Cincinnati Children's Hospital Medical Center and the University of Minnesota approved the experiments and confirmed that all experiments conform to the relevant regulatory standards.

METHOD DETAILS

Immunostaining

For frozen sections, OCT was removed by incubation with 1XPBS. We permeabilized cells in ice cold MeOH for 10 min., followed by incubation in normal donkey serum (Jackson ImmunoResearch Cat# 017–000-121) and 0.3% Triton-X100 (Sigma-Aldrich Cat# X100). Primary antibody incubation occurred overnight at 4 degree Celsius with the following antibodies: Anti-Glut1 antibody (1:300, Abcam, Cat#ab115730), Fibrinogen antibody (1:500, Agilent DAKO, Cat#: A008002-2), CD31 antibody (1:100, BD Biosciences, Cat#: 553370), pPKA antibody (1:200, Cell Signaling, Cat#: 9621S), Cav1 antibody (1:400, Cell Signaling, Cat#:3238S), CD45 antibody (1:300, Novus Biologicals, Cat# 100-77417), β-galactosidase polyclonal antibody (1:1000, Thermo Fisher, Cat#: A-11132), anti-Iba-1 (1:3,000, Wako Chemicals, Cat#: 019-19741), Claudin-5 polyclonal antibody (1:100, ThermoFisher Scientific, Cat# 341600), ZO-1 polyclonal antibody (1:100, ThermoFisher Scientific, Cat#: 402200). All secondary antibodies were donkey anti Rat/Rabbit/Goat from Jackson ImmunoResearch, reconstituted in 50% glycerol and used at 1:250 dilution. To visualize nuclei, sections were stained with DAPI for 10min., washed with PBS and mounted in FluoromountG (Electron Microscopy Sciences, Hatfield, PA). Images were acquired with NIS-Elements software using confocal microscopy (Nikon). Images were analyzed using ImageJ. For staining paraffin sections, tissue samples were formalin fixed, paraffin embedded and cut into 5um sections. Hematoxylin and Eosin (H&E) staining (Thermo Fisher Scientific, 7221 and 7111), was performed according to manufacturer's instructions.

IgA and alpha 2 Macroglobulin immunohistochemistry

Sections were deparafinized, hydrated and processed for antigen retrieval using citrate buffer (ph 6.00). Sections were washed, processed for IHC using mouse IgA antibody from Cell Signaling (Cat # 50384) at a dilution of 1:800 and rabbit alpha 2 macroglobulin from Cell Signaling (Cat # 71610) at a dilution of 1:500 Overnight. Sections were washed and treated with biotinylated Goat anti-mouse antibody for IgA and

biotinylated Goat anti Rabbit antibody for alpha macroglobulin (Vector) at a dilution of 1:200. After PBS wash, sections were treated with ABC (Vector), washed and stained with and DAB (Vector).

Electron microscopy

Mice were perfusion fixed with 4% paraformaldehyde and 2.5% glutaraldehyde in 0.1-M phosphate buffer at 7.4 pH. Saphenous nerve was dissected out and postfixed overnight, then transferred to 0.175 mol/L cacodylate buffer, osmicated, dehydrated, and embedded in Embed 812 (Ladd Research Industries). Ultrathin sections were stained in uranyl acetate and lead citrate and viewed on a Hitachi H-7600 microscope.

CNPAse-hEGFR Cav1 mice protocol

For CNPase-hEGFR transgenic mice, tissue analysis consisted of at time of necropsy, sciatic nerves and individual paraspinal dorsal root ganglion were carefully removed under a dissecting microscope (Leica Microsystems Inc.), washed, and placed in cold PBS. Tissues were imaged at 2.5x objective and measurements were taken. Paraffin sections were prepared and stained as described above.

RNA sequencing

For polyA stranded RNA sequencing (n=2) per genotype, total RNAs isolated from wildtype, P2RY14-/-; Nf1fl/fl; Dhh+ and P2RY14-/- Nf1fl/fl; Dhh+ mouse sciatic nerves were amplified using the Illumina NovaSeq600 (Illumina Technologies) according to manufacturer's protocol and CCHMC DNA sequencing and Genomic Core protocol. Base calling was performed using Illumina CASAVA (v1.4) and the quality of sequencing reads was checked using FASTQC (v0.11.7,https://www.bioinformatics.babraham.ac.uk/projects/fastqc). Reads were aligned against mm10 mouse genome using HISAT2 (v2.0.5, http://www.ccb.jhu.edu/software/hisat/index.shtml). Raw gene counts were calculated using featureCounts (v1.5.2, http://subread.sourceforge.net) and normalized using edgeR (https://bioconductor.org/packages/release/bioc/html/edgeR.html)'s TMM (trimmed mean of M values) method. The RNAseq data discussed in this publication have been deposited in NCBI's Gene Expression Omnibus[71] and are accessible through GEO series accession number GSE189189.

Osmotic pump drug study

4-month-old neurofibroma mice (Nf1 fl/fl Dhh+) were treated with the P2RY14 inhibitor (PPTN-HCl:4-[4-(4-Piperidinyl]-7-[4-(trifluoromethyl) phenyl]-2-naphthalenecarboxyliv acid hydrochloride) (TOCRIS: Cat #. 4862). Osmotic minipumps were loaded with the P2RY14 inhibitor drug according to manufacturer's instructions with PPTN in saline solution (containing DMSO) or with saline containing equivalent amounts of the vehicle control (DMSO). Osmotic minipumps released the inhibitor hourly for 14 days for a daily dose of 4.55 mg/kg. At day 14, mice were perfusion fixed with 4% paraformaldehyde and used a Leica dissecting microscope to dissect the tissue.

QUANTIFICATION AND STATISTICAL ANALYSIS

Statistical parameters, including the statistical tests used, exact value of the number of samples (*n*), what (*n*) represents, and descriptive statistics and significance are reported in the figures and figure legends. Two-group comparisons used Student's t-tests. When multiple genotypes were analyzed in a single experiment, we used a one-way ANOVA with multiple comparisons. All data unless otherwise stated is represented as average $\pm$ SD and was analyzed in GraphPad Prism 7. For the quantification of TJs, caveolae, perineurial layers and perineurial width, the mean number of TJs and caveolae for all genotypes was counted directly from the electron microscopy montage per field of view using images at 20,000X. The mean number of perineurial layers for all groups was counted directly form the electron microscopy montage using images at 5,000X magnification. The width of the perineurium of each nerve was quantified using ImageJ and was measured directly from the electron microscopy montage using images at 10,000X magnification. All measurements were plotted using GraphPad Prism.